Virology 464-465 (2014) 385–396

Contents lists available at ScienceDirect

Virology

journal homepage: www.elsevier.com/locate/yviro

Characterization of Coffee ringspot virus-Lavras: A model for an emerging threat to coffee production and quality

T.O. Ramalho [b], A.R. Figueira [b], A.J. Sotero [b], R. Wang [a], P.S. Geraldino Duarte [b], M. Farman [a], M.M. Goodin [a,*]

[a] Department of Plant Pathology, University of Kentucky, Lexington, KY 40546, USA
[b] Universidade Federal de Lavras, Departamento de Fitopatologia, Caixa Postal 3037, CEP 37200-000 Lavras, MG, Brasil

ARTICLE INFO

Article history:
Received 16 June 2014
Returned to author for revisions
24 June 2014
Accepted 19 July 2014
Available online 9 August 2014

Keywords:
Dichorhavirus
Rhabdovirus
Protein localization
Climate change
Negative-strand RNA virus
Brazil
Virus emergence

ABSTRACT

The emergence of viruses in Coffee (*Coffea arabica* and *Coffea canephora*), the most widely traded agricultural commodity in the world, is of critical concern. The RNA1 (6552 nt) of Coffee ringspot virus is organized into five open reading frames (ORFs) capable of encoding the viral nucleocapsid (ORF1p), phosphoprotein (ORF2p), putative cell-to-cell movement protein (ORF3p), matrix protein (ORF4p) and glycoprotein (ORF5p). Each ORF is separated by a conserved intergenic junction. RNA2 (5945 nt), which completes the bipartite genome, encodes a single protein (ORF6p) with homology to RNA-dependent RNA polymerases. Phylogenetic analysis of L protein sequences firmly establishes CoRSV as a member of the recently proposed Dichorhavirus genus. Predictive algorithms, *in planta* protein expression, and a yeast-based nuclear import assay were used to determine the nucleophillic character of five CoRSV proteins. Finally, the temperature-dependent ability of CoRSV to establish systemic infections in an initially local lesion host was quantified.

Introduction

In descending order of value, the four most widely traded global commodities are petroleum, coffee, natural gas and gold. As such, coffee is the most widely traded agricultural commodity in the world. Per capita consumption worldwide is approximately half a cup per day. To meet this demand, coffee-producing countries exported some 7.9 million metric tons of coffee beans in 2010, with an estimated value of USD $15.4 billion, with processing and distribution increasing this value many-fold. The consumption of coffee is entrenched culturally around the world, with over 10,000 cafes in the United States alone. Although grown commercially in most tropical and subtropical countries, the world supply of coffee is dominated by Brazil, which produces 35% of the global exports of green coffee beans. As such, the emergence of Coffee ringspot virus (CoRSV), which is transmitted by the tenuipalpid mite *Brevipalpus phoenicis*, is of critical concern (Chagas et al., 2003a; Figueira, 2008). The transmission of CoRSV by *B. phoenicis* as well as its preliminary characterization linked it taxonomically to orchid fleck virus (OFV) and citrus leprosis virus, nuclear type (CiLV-N) which are presently unassigned negative-sense, single-stranded RNA plant-adpated viruses that were previously proposed to be included in the family *Rhabdoviridae*, and order *Mononegavirales* (Kitajima et al., 2003b; Kondo et al., 2006). The taxonomic placement of these viruses is equivocal at present as OFV has a bipartite genome, which is encapsidated in particles that are not enveloped. Thus, OFV and related viruses cannot be included in the *Mononegaviriales*, under its present defining criteria (Kondo et al., 2006, 2009). It has been proposed, therefore, that these viruses can be classified taxonomically in new species in a new free-floating genus Dichorhavirus (Dietzgen et al., 2014).

CoRSV was first reported on *Coffea arabica* plants in Brazil in 1938 (Bittancourt, 1938). The disease is characterized by the appearance of its namesake ring-shaped lesions on leaves that eventually become chlorotic before falling prematurely from plants (Almeida et al., 2012; Bittancourt, 1938; Chagas et al., 2003a). Symptoms may also appear on coffee cherries, which develop chlorotic or necrotic lesions that are frequently invaded by secondary fungal or bacterial opportunists. Even in cases where the overall yield of CoRSV-infected plants is not affected by more than a few percent, scalding of cherries exposed to the sun due to virus-induced defoliation and subsequent secondary infections can severely impair the drinking quality of the coffee, which in turn translates into a marked devaluation of the harvested cherries (Bertrand et al., 2012).

Although the impact of CoRSV is of greatest concern in Brazil, this virus has been reported to occur in other major coffee-growing regions including Costa Rica (Almeida et al., 2012; Chagas et al., 2003a; Kitajima et al., 2011). The expansion of CoRSV

* Corresponding author.
E-mail address: mgoodin@uky.edu (M.M. Goodin).

http://dx.doi.org/10.1016/j.virol.2014.07.031

in Minas Gerais (MG) state of Brazil, which itself accounts for approximately 17% of global green coffee bean exports and 50% all of Brazilian coffee, was the primary motivation for this study. Field surveys have established that CoRSV is increasingly prevalent in the major coffee production areas of MG and adjacent states (Almeida et al., 2012; Figueira, 2008). Quite possibly, the emergence of CoRSV may be exacerbated by its residency in weedy species during the August through April period when *B. phoenicis* populations are lowest (De Carvalho Mineiro et al., 2008). Effective weed sanitation may be suppressed during periods of low economic return for coffee, a factor that may further compound CoRSV emergence. This situation may be truly significant, if CoRSV is also found in populations of *Commelina benghalensis* L, which have been found to harbor the *Brevipalpus sp.*-transmitted citrus leprosis-associated virus, Cytoplasmatic type (CiLV-C) (Nunes et al., 2012). Collectively, biological, environmental and economic factors are combining to drive emergence of CoRSV. For these reasons the molecular characterization of the Lavras strain of CoRSV was undertaken in order to develop a research model for coffee ringspot disease.

CoRSV was tentatively assigned to the family *Rhabdoviridae* based upon earlier reports of bacilliform particles in the ranges of 59–76 nm in diameter and 178–224 nm in length in nuclei and perinuclear endoplasmic reticulum (ER) of infected cells (Ito et al., 2013; Kitajima et al., 2003a). In addition, the first fragment of CoRSV-derived sequence (GenBank: GQ979998.1) further supported inclusion of this virus within the *Mononegavirales*, based upon its relation to polymerases encoded by viruses in this group. In order to resolve the taxonomic assignment of CoRSV and to generate resources for the molecular and cellular biology studies, we employed a next-generation sequencing approach, which is now firmly established as the first strategy for identification and characterization of genetically diverse emerging viruses (Coetzee et al., 2010; Grard et al., 2012; Idris et al., 2014; Ito et al., 2013; Vives et al., 2013).

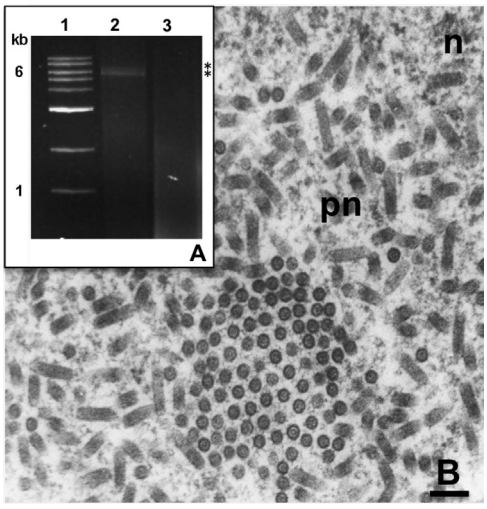

Fig. 1. (A) Electrophoretic analysis of RNAs extracted from semi-purified CoRSV preparations isolated from systemically infected *C. quinoa*. Lane 1. 1 kb molecular weight marker DNAs, which are used here on non-denaturing agarose gels just to provide general estimation of size. The exact size of the genome was determined by RNA sequencing. Lane 2. RNA extracted from semi-purified virus. Lane 3. RNA isolated from preparations from mock-inoculated plants. (B) Transmission electron micrograph of a thin section of *C. quinoa* leaf tissue infected with CoRSV. Bar = 100 nm. The granular chromatin of the nucleus (**n**) is labeled to differentiate it from the perinuclear regions (**pn**), where viral particles accumulate.

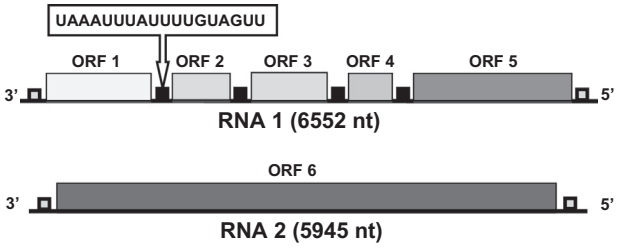

Fig. 2. Organization of the CoRSV genome. The bipartite genome encodes five open reading frames (ORFs) on RNA1 (6552 nt) and a single ORF on RNA2 (5945 nt). The ORFs are separated by conserved gene junctions (black squares), except at the 3′ and 5′ termini, where the gene junctions are truncated to transcription start sites or poly-adenylation signals, respectively (open squares). The consensus gene junction is shown between ORFs 1 and 2.

Results

Virion morphology and genomic RNA analysis of CoRSV

Electrophoretic analysis in non-denaturing agarose gels demonstrated the presence of two high-molecular weight RNAs of about 6 kb each in RNA preparations extracted from semi-purified virions (Fig. 1A). Examination of thin sections of CoRSV-infected tissue by electron microscopy revealed the presence of bacilliform particles in the nucleus and perinuclear regions of cells. These particles were arranged seemingly at random or in paracrystalline arrays. As reported previously, particle sizes were in the range of 45 nm × 110–145 nm (Fig. 1B) (Chagas et al., 2003b; Dietzgen et al., 2014; Kitajima et al., 2003a).

Organization of the CoRSV genome

Assembly of the RNA-Seq data into contigs was performed using the Trinity program (Haas et al., 2013). The data was processed using 25 nt as the minimal overlapping lengths (k-mer), which yielded 19,819 contigs of 201–3607 nt. Searches using BLASTN and BLASTX detected two clusters of contigs having detectable sequence identity to known viral RNA sequences. One cluster of contigs showed the lowest *e*-values with the RNA-dependent RNA polymerases. This cluster was ultimately determined to be CoRSV RNA2. A second cluster had low *e*-values in matches with phosphoproteins, glycoproteins and nucleocapsid proteins of several rhabdoviruses, as well as OFV. RACE and additional Sanger sequencing established this second cluster as CoRSV RNA1.

Following assembly and secondary sequencing, the complete genome of CoRSV was found to consist of 6552 nt in RNA1 and 5945 nt in RNA2. These sequences have been deposited into Genbank as accessions KF812525.1 and KF812526.1, respectively. In contrast to earlier speculation that CoRSV was a rhabdovirus, sequence determination confirmed the bipartite nature of the CoRSV genome, similar to those of OFV and others species in the recently proposed Dichorhavirus genus (Fig. 2) (Dietzgen et al., 2014).

The sequence of RNA1 has coding capacity for five ORFs, while RNA2 encodes only a single large ORF. RNA1 is flanked by a 60 nt long 3′ leader and a 134 nt 5′ trailer. Similarly, RNA2 is flanked by a 131 long 3′ leader and a 136 nt trailer. There is only 21% and 47% base complementarity between the leader and trailer termini of RNAs 1 and 2, respectively (data not shown).

Gene junctions in the CoRSV genome

A consensus gene junction, 3′–UAAAUUUAUUUU GUA GUU–5′, is located between each ORF on RNA1 (Fig. 3). This junction is typical of that for rhabodviruses in that it is organized into three

	1	2	3
ldr/OFR1		GU**G**	GUU
ORF1/ORF2	UAAAUUUAUUUU	GUA	GUU
ORF2/ORF3	UAAAUUUAUUUU	GUA	GUU
ORF3/ORF4	UAAAUUUAUUUU	GUA	GUU
ORF4/ORF5	UAAAUUUAUUUU	GU**G**	GUU
ORF5/trl	UAAAUUU**G**UUUU	G	
ldr/ORF6		GUA	GUU
ORF6/trl	UAAAUU**AG**UUUU	G	
Consensus	**UAAAUUUAUUUU**	**GUA**	**GUU**

Fig. 3. Sequence of each intergenic junction (IGJ) in the CoRSV genomic RNA. The IGJs are divided into three sections to denote the (1) poly-adenylation signal, (2) intergenic spacer and (3) transcription start site. The consensus IGJ is provided at the bottom. Nucleotides in individual IGJs that are variant from the consensus are shown in bold.

		1	2	3
D	CoRSV/RNA1	UAAAUUUAUUUU	GUA	GUU
	CoRSV/RNA2	UAAAUUA	GUU	UUG
	OFV/RNA1	UAAAUUUAUUUU	GUUG	UU
	OFV/RNA2	UAAAUUUCUUUU	GUUG	GUU
N	PYDV	UUAUUUUU	GGG	UUG
	MFSV	UUUAUUUU	GUAG	UUG
	SYNV	AUUCUUUUU	GG	UUG
	MMV	AAUUCUUUUU	GGG	UUG
	RYSV	AUUCUUUUU	GGG	UUG
	TaVCV	AAUUCUUUUU	GGG	UUG
C	LNYV	AUUCUUUU	G(N)$_n$	CUA
	NCMV	AUUCUUUUU	GACU	CUA
V	VSIV	ACUUUUUUU	GU	UUG

Fig. 4. Comparison of consensus intergenic junction (IGJ) sequences in RNAs 1 and 2 for the dichorhaviruses (D) orchid fleck virus (OFV) and Coffee ringspot virus (CoRSV) with the consensus IGJs from selected rhabdoviruses in the *Nucleorhabdovirus* (N), *Cytorhabdovirus* (C) or *Vesiculovirus* (V) genera. The IGJs are divided into three sections to denote the (1) poly-adenylation signal, (2) intergenic spacer and (3) transcription start site. Abbreviations for the viral names included here are defined in Section 4.

modules; a 3′ poly-adenylation signal (Module 1), three non-templated nucleotides (Module 2) and a transcription initiation sequence (Module 3) (Jackson et al., 2005). The poly(A)$^+$ signal is composed of 12 nts that have an invariant UAAAUU sequence followed by two bases that are either UA or UG with their respective untranslated regions (UTRs) of each mRNA. These variant residues are followed by a run of four uridine residues to complete the poly(A)$^+$ signal. A similar signal sequence (3′–UAAAUUUAUUUU) is present in ORF6 flanking region on RNA2. The non-templated nucleotides are either GUA or GUG, which are followed by an invariant GUU transcription start site. The ldr/ORF1 and ldr/ORF6 junctions on RNA1 and RNA2, respectively, lack the Module 1 poly(A)$^+$ signal. Similarly, the ORF5/trl and ORF6/trl junctions lack the Module 3 transcription start sites.

The Module 1 sequences for RNA1 of CoRSV and OFV are identical. However, Modules 2 and 3 differ slightly, with Module 2 being GUA in CoRSV compared to GUUG in OFV and Module 3 being GUU in CoRSV and UU in OFV. The Module 1 sequences of both CoRSV and OFV are longer by four uridine residues relative to plant-adapted rhabdoviruses such as PYDV, SYNV, MFSV, LNYV and others (Fig. 4) (Bandyopadhyay et al., 2010; Tsai et al., 2005; Wetzel et al., 1994).

Characteristics of proteins encoded in the CoRSV genome

Several algorithms were used to predict functional domains in the primary structure for proteins corresponding to each ORF in the CoRSV genome (Bendtsen et al., 2004; Blom et al., 1994, 2004; Gasteiger et al., 2003; Nakai and Kanehisa, 1991, 1992). A subset of this information is provided in Table 1. Five ORFs are predicted on RNA1. ORF1 likely encodes the CoRSV nucleocapsid protein, with a predicted molecular weight of 49 kDa (pI=5.8). All tested algorithms failed to identify a putative nuclear localization signal (NLS) in this protein although two putative nuclear export signals (NESs), ^{77}LLIIMSL^{85} and ^{249}LILQHMDL^{258} were predicted in this protein. ORF 2 is likely to encode the phosphoprotein for CoRSV with a molecular weight of 27 kDa (pI=6.7). This protein contains two predicted NLSs, ^{127}PMKRST^{134} and ^{230}KKKKR^{235}, in the primary structure of the protein. Like ORF1p, ORF2p also contains a putative NES, ^{194}LPSLLGDITI^{205}. A 36 kDa (pI=8.74) protein with homology to viral cell-to-cell movement proteins could be encoded by ORF 3. As with the ORF 1 protein, no NLSs were predicted in this protein, but an NES was found, ^{107}LATSGVLKLSI^{119}. ORF4 has the capacity to encode a 20 kDa basic protein (pI=9.27), and likely encodes the CoRSV matrix protein given the similar gene order to OFV (Kondo et al., 2009). Interestingly, the ORF4 protein has a predicted NLS between residues ^{152}KRPR^{156} in its primary structure. The ORF5 protein, with a predicted molecular weight of 60 kDa (pI=6.16), contains hallmarks of a Type 1 integral membrane protein including a transmembrane domain at amino acids 490–506 and a signal peptide cleavage site at residue 34 from the amino terminus. Consistent with the requirement to be targeted to the inner nuclear membrane, the ORF5 protein has a predicted NLS (^{200}PRCKRRV^{206}). Together with additional information from protein identity searches (data not shown), these data suggest that ORF5p is the CoRSV glycoprotein. The antigenomic RNA of CoRSV RNA2 contains a single ORF capable of encoding a protein of 212 kDa (pI=7.43). Homology searches suggest that this protein in likely the CoRSV RNA-dependent RNA polymerase. Contained in the primary structure of this protein is an NLS ^{390}KKHK^{394} as well as an NES ^{111}LNLTEEELPL^{122}. Protein alignment of the predicted CoRSV polymerase with that of other negative-strand RNA viruses identified four highly conserved motifs (Fig. 5, Motifs A–D), consisting of seven invariant regions (Bourhy et al., 2005). As expected for polymerase sequences, these motifs are highly-conserved within the dichorhaviruses, with the greatest divergence being in Motif D (Fig. 5).

Relationship of CoRSV to other negative-strand RNA viruses

Phylogenetic relationships among negative-strand RNA viruses were assessed using the nucleocapsid and polymerase proteins of CoRSV and related viruses. As the results were similar, only those for the polymerase are included here. Akin to that established using sequences from OFV and CiLV-N, the clade containing the bipartite dichorhaviruses shows a relationship most closely aligned with viruses in the genus *Nucleorhabdovirus* (Fig. 6). In contrast to the close relatedness of OFV and CiLV-N, CoRSV overall sequence identity of 70% to OFV suggests that these are truly distinct viruses and not virus strains (Dietzgen et al., 2014).

Subcellular localization of CoRSV proteins

As demonstrated previously for negative-strand RNA viruses, subcellular localization of viral proteins is frequently difficult to

Table 1
Features of CoRSV proteins determined by predictive algorithms. NLS = nuclear localization signal. NES = nuclear export signal. Location of amino acid residues in the primary structure of proteins is provided in superscript.

ORF	MW (kD)	Isoelectric point	Predicted NLS	Predicted NES	Putative function	Highest scoring virus/*e*-value
1	49	5.8	None	^{77}LLIIMSL^{85} ^{249}LILQHMDL^{258}	Nucleocapsid protein	OFV/$1e^{-151}$
2	27	6.7	^{127}PMKRST^{134} ^{230}KKKKR^{235}	^{194}LPSLLGDITI^{205}	Phosphoprotein	OFV/$7e^{-36}$
3	36	8.74	None	^{107}LATSGVLKLSI^{119}	Movement	OFV/$2e^{-135}$
4	20	9.27	^{152}KRPR^{156}	None	Matrix protein	OFV/$2e^{-42}$
5	60	6.16	^{199}PRCKRRV^{207}	None	Glycoprotein	OFV/$4e^{-89}$
6	212	7.43	^{390}KKHK^{394}	^{111}LNLTEEELPL^{122}	Polymerase	OFV/0.0

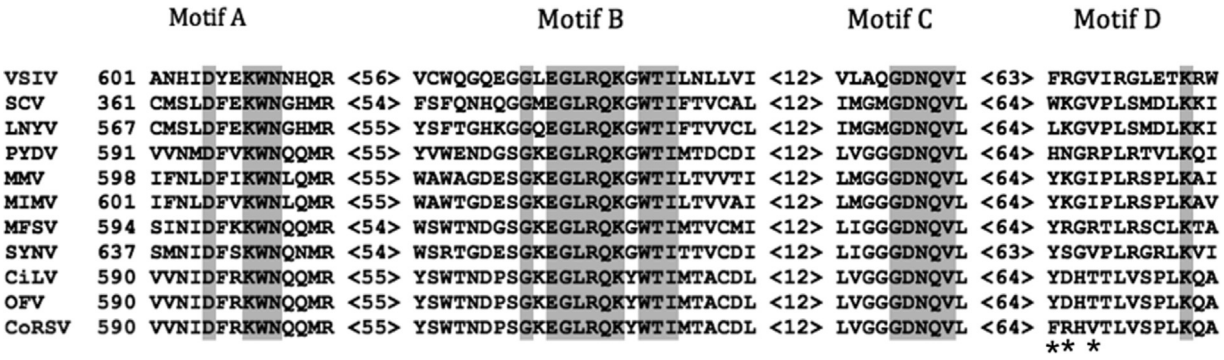

Fig. 5. Amino acid alignment of conserved blocks within RNA-dependent RNA polymerases encoded by rhabdoviruses and dichorhaviruses. Conserved residues are highlighted in gray. Species names are defined in Section 4. Asterisks indicate amino acid residues in the CoRSV polymerase that are most divergent compared to other dichorhaviruses.

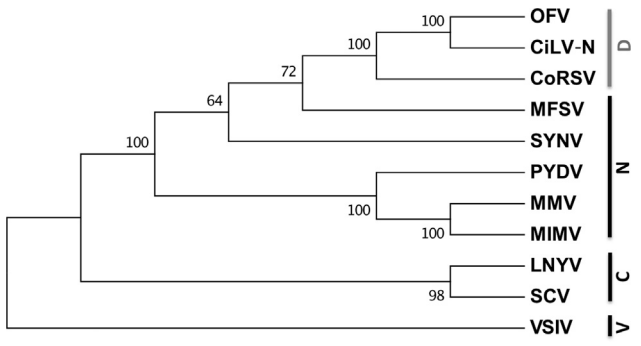

Fig. 6. Phylogeny of rhabdoviruses (bold black bars) and members of the proposed Dichorhavirus genus of bipartite *Brevipalpus*-transmitted viruses (bold gray bar) inferred from polymerase protein sequences. Representative nucleorhabdoviruses (N) and cytorhabdoviruses (C) infecting diverse host plants are used here, as well as *Vesicular stomatitis Indiana virus* (V), representing non-plant-adapted viruses. Bootstrap values greater than 50% are shown at nodes in the tree. Virus names and Genbank accession numbers for their sequenced genomes are listed in Section 4.

determine strictly from *in silico* methods (Bandyopadhyay et al., 2010). Therefore, we utilized an established strategy for protein localization using an *Agrobacterium*-mediated transient expression of fluorescent protein fusions in transgenic *Nicotiana benthamiana* lines that express subcellular markers. At first step we expressed the CoRSV ORF 1–5 proteins as amino or carboxy-terminal fusions to GFP in transgenic plants expressing a red nuclear marker (Anderson et al., 2012; Bandyopadhyay et al., 2010). Only a subset of these data are provided here. The GFP-ORF1p fusion (~77 kDa) could be detected at steady state in both the nucleus and the cytoplasm in a pattern indistinguishable from GFP alone, despite the fact that this fusion is over the size exclusion limit for plant nuclear pore complexes (Fig. 7 panels 1A–F vs 7A–F). In marked contrast, the GFP-ORF2p fusion localized exclusively to the nucleus (Fig. 7 panels 2A–F). Consistent with a predicted function as a cell-to-cell movement protein, the GFP-ORF3p fusion accumulated predominantly at the cell periphery (Fig. 7 panels 3A–F). GFP-ORF4p accumulated in the nucleus but could also be found as cytoplasmic aggregates (Fig. 7 panels 4A–F). GFP-ORF5p was targeted to the nuclear envelope and, to a lesser extent, perinuclear membranes (Fig. 7 panels 5A–F and 6A–F).

Previous reports have established firmly that coexpression of proteins encoded by negative-strand RNA viruses can alter their localization patterns relative to when they are expressed alone (Goodin et al., 2001; Tsai et al., 2005). This relocalization has been mostly interpreted in terms of establishing viroplasms, the site of replication and nucleocapsid condensation (Deng et al., 2007; Ghosh et al., 2008; Kondo et al., 2013; Martin et al., 2012). In order to investigate this phenomenon for CoRSV, we used both coexpression and BiFC. As BiFC tends to provide insight into the localization of the most stable protein complex (Kerppola, 2008), we used this assay to examine further the ORF1p and ORF2p interaction, and that of other CoRSV proteins (Fig. 8). These assays suggest that the most stable ORF1p/ORF2p complexes reside within a sub-nuclear locale (Fig. 8 1A–F). Similar to the localization of its GFP fusion, the ORF2p/ORF2p interaction was exclusively nuclear. In contrast to the ORF1p/ORF2p interaction, the homologous interaction of ORF2p exhibited uniform distribution throughout the nucleoplasm and exclusion from what appears to be the nucleolus. Interaction of the ORF1p and ORF4p proteins was detected within the perinuclear region. A similar localization pattern was also produced by the ORF5p/ORF5p interaction, which is expected of glycoproteins of nucleorhabdoviruses (Gaudin et al., 1992; Kreis and Lodish, 1986; Whitt et al., 1991; Wilcox et al., 1992). Finally, the ORF2p/ORF4p interaction was exclusively nuclear (Fig. 8 panels 5A–F). There was no positive interaction noted for ORF3p/ORF1p or any other combination of proteins, see those discussed above. Likewise, none of the CoRSV proteins interacted with glutathione-s-transferase (GST) or maltose-binding protein (MBP) in BiFC assays used as negative controls

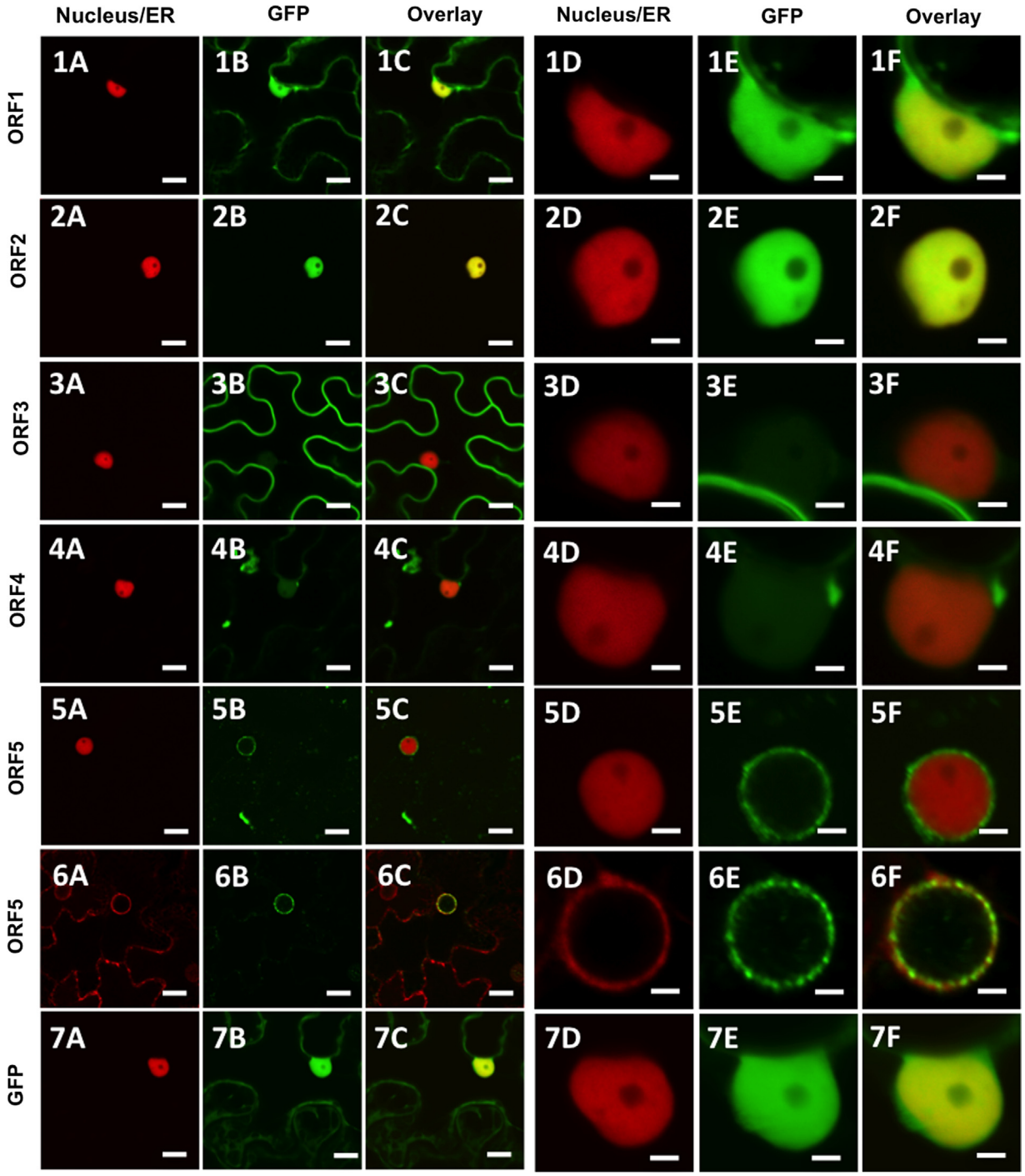

Fig. 7. Confocal micrographs of CoRSV protein fusions expressed by agroinfiltration in leaf epidermal cells of transgenic *N. benthamiana* plants expressing RFP fused to histone 2B, a nuclear marker (Nucleus; panels 1–5 and 7) or targeted to the endoplasmic reticulum (panel 6). Whole cell (panels A–C, scale bar = 10 μm) or nuclear (panels D–F, scale bar = 2 μm) views of fluorescence of GFP, RFP and overlaid images, respectively, are provided. (1A–F) CoRSV ORF1p-GFP. (2A–F) CoRSV ORF2p-GFP. (3A–F) CoRSV ORF3p-GFP. (4A–C) CoRSV ORF4p-GFP. (5A–F) CoRSV ORF5p-GFP. (6A–F) CoRSV ORF5p-GFP localized in RFP-ER plants. In these panels only the ring of the nuclear envelope can be seen, compared to chromatin-containing areas observed in other RFP panels shown here. (7A–F) GFP. Images are acquired two days post-agroinfiltration.

(Anderson et al., 2012; Bandyopadhyay et al., 2010; Min et al., 2010).

Relocalization of ORF2p to the cytoplasm by ORF1p

As noted above, association of the nucleocapsid (N) proteins and phosphoproteins (P) of negative-strand RNA viruses is a key element in the formation of viroplasma, where replication takes place. As such, many N/P interactions have been mapped or characterized to various degrees (Deng et al., 2007; Goodin et al., 2001; Kondo et al., 2013). In addition to viroplasm formation, nuclear-localized viruses are faced with the additional challenge that they need to export nucleocapsids from the nucleus in order to establish infections in adjacent cells (Cros and Palese, 2003; Elton et al., 2001; Min et al., 2010; O'Neill et al., 1998). Thus, we investigated the differential localization patterns for ORF1p and ORF2p expressed independently or together in plant cells. Surprisingly, and in contrast to the BiFC experiments, we found that

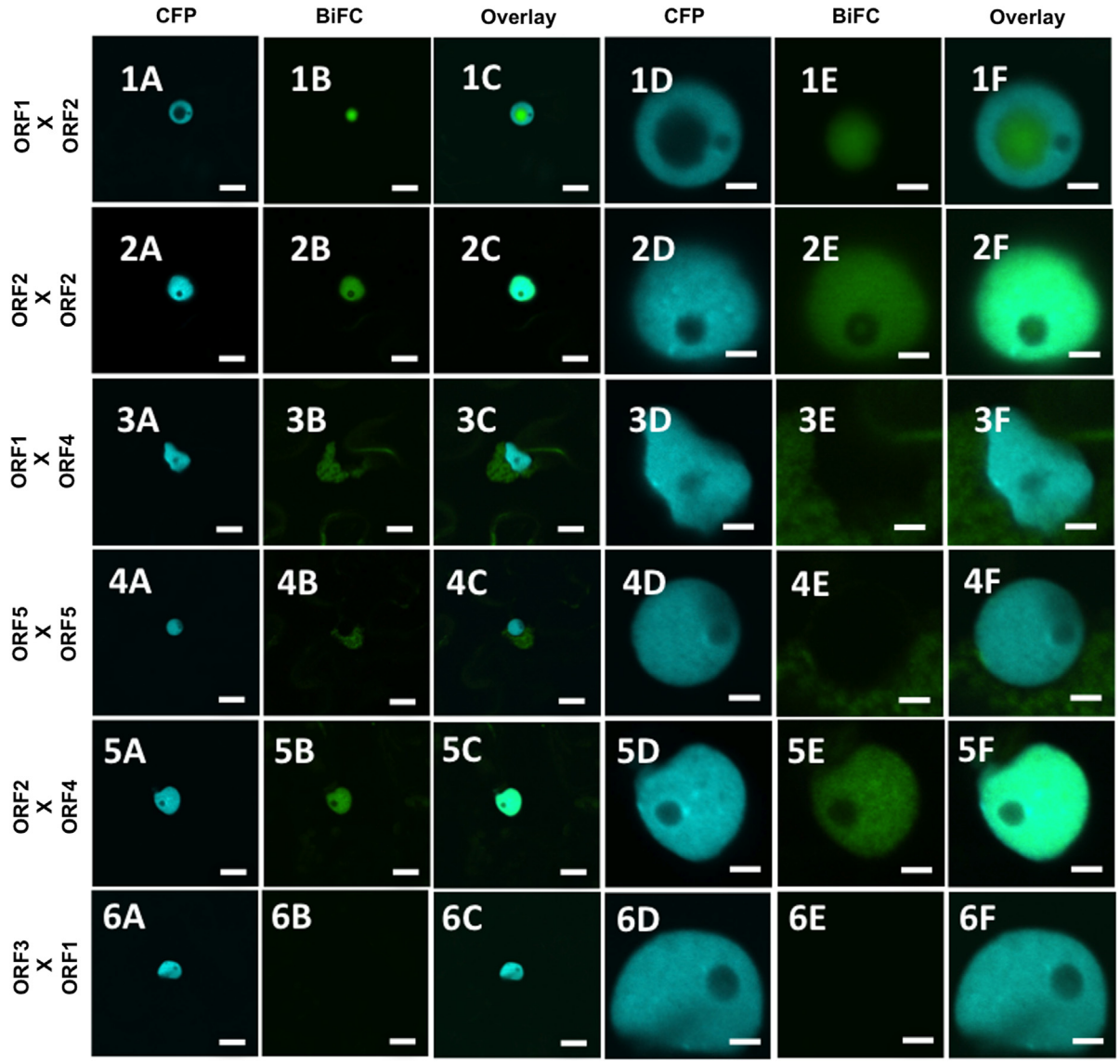

Fig. 8. Single-section confocal micrographs showing relocalization of CoRSV proteins when coexpressed, as determined by BiFC, which characteristically shows localization of the most stable of possible protein interactions. Coexpression assays are conducted in leaf epidermal cells of transgenic *N. benthamiana* expressing cyan fluorescent protein (CFP) fused to the nuclear marker Histone 2B (CFP-H2B). Shown in panels A, B and C are micrographs of CFP, YFP (BiFC) fluorescence and the resultant overlay, respectively (scale bar = 10 μm). Panels D–F are corresponding nuclear views (scale bar = 2 μm) of the cell shown in panels A–C. Proteins listed first in the pair of interactors are expressed as fusions to the amino-terminal half of YFP. Those listed second are expressed as fusions to the carboxy-terminal half of YFP. However, protein fusions to each half of YFP are tested in all pairwise interactions of which a subset is shown here. Glutathione-S-transferase serves as a non-binding control that does not interact with itself. (1A–F) ORF1p X ORF2p. (2A–F) ORF2p X ORF2p. (3A–F) ORF1 X ORF4. (4A–F) ORF 5p X ORF 5p. (5A–F) ORF2p X ORF4p. (6A–F) ORF3p X ORF1p, shown here to demonstrate a negative BiFC assay.

coexpression of these two proteins resulted in a relocalization of ORF2p to the cytoplasm, despite the observation of it being entirely nuclear-localized when expressed alone (Fig. 9, Panels 1–3 A–C). Control experiments confirmed that this relocalization was entirely dependent upon the presence of both ORF1p and ORF2p since neither of the fusions partners, GFP or RFP, influenced the localization patterns (Fig. 9, Panels 4–6 A–C).

Nuclear import of CoRSV protein in yeast

The *in silico* prediction and *in planta* localization experiments were further supported by a third method to determine nuclear import of proteins (Fig. 10). In this assay, only proteins containing a functional NLS can facilitate the nuclear import of a transcriptional activator required for the expression of a reporter gene in yeast cells, which permits yeast to grow on minimal media lacking histidine (Bandyopadhyay et al., 2010; Zaltsman et al., 2007). Entirely consistent with the *in planta* localization data all CoRSV-encoded proteins, with the exception of ORF3p, tested positive in the NIA. Yeast cells expressing the NIA-ORF 2p fusion exhibited the most robust growth, which may indicate the strength of the two predicted NLSs in this protein, given that it was also entirely localized to the nucleus when expressed as GFP or RFP fusions in plant cells. ORF4p also conferred strong growth in yeast cells, with growth of cells comparable to those expressing the histone 2b positive control (Fig. 10, compare lanes 1 and 4). ORF5p, the putative CoRSV glycoprotein was also NIA positive. Finally, ORF1p showed the weakest positive response in the NIA, consistent with the fact that GFP fusions of this protein partitioned between the nucleus and cytoplasm in plants. We note here that the NIA data are qualitative and that the ability of yeast to grow on dropout media may not in fact be an indicator of the strength of NLSs in particular proteins.

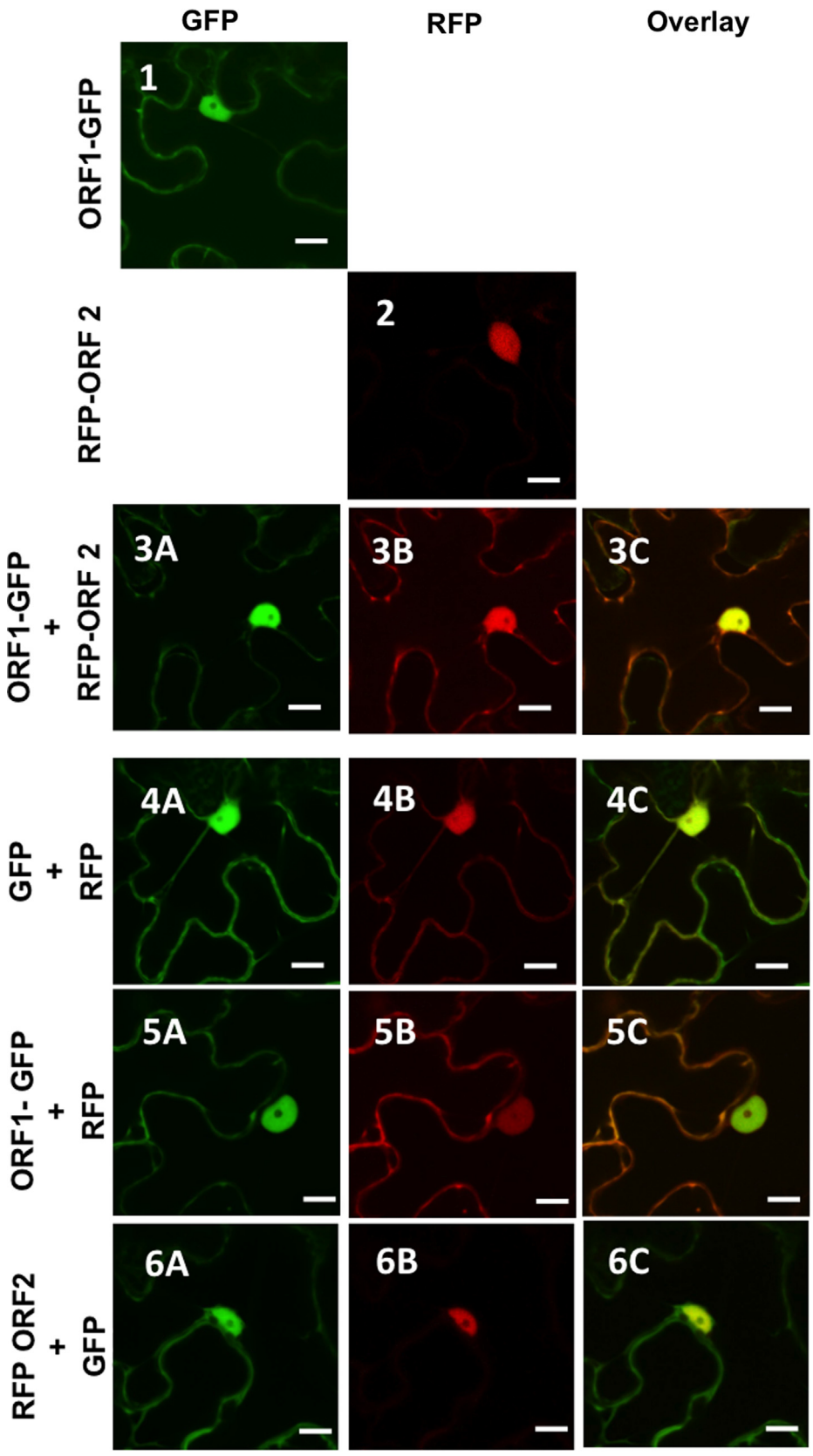

Fig. 9. Confocal micrographs of CoRSV protein fusions expressed by agroinfiltration in leaf epidermal cells of wild-type *N. benthamiana* plants. Whole cell (scale bar = 10 μm) views of fluorescence of GFP (A), RFP (B) and overlaid (C) images are provided to demonstrate relocalization of some ORF2p from the nucleus to the cytoplasm when expressed in the presence of ORF1p. (1A) CoRSV ORF1p-GFP. (2A) CoRSV RFP-ORF2p. (3A–F) CoRSV ORF1p-GFP and CoRSV RFP-ORF2p. (4A–C) GFP and RFP. (5A–F) CoRSV ORF1p-GFP and RFP. (6A–F) GFP and CoRSV RFP-ORF2p. Images are acquired two days post-agroinfiltration. The most stable orientations of autofluorescent protein fusions are employed in this experiment to facilitate detection by confocal microscopy.

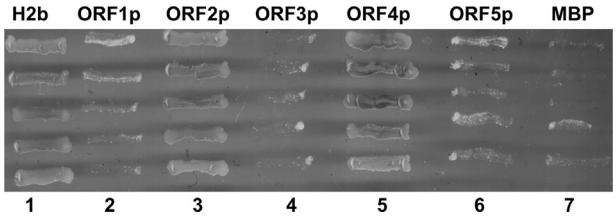

Fig. 10. Yeast-based assay for identification of proteins containing a functional NLS. Positive- (Lane 1; H2B) and negative-control (Lane 7; MBP) proteins or CoRSV proteins (Lanes 2–6; ORF1p-ORF5p) are expressed from pNIA-DEST in yeast strain L40. Only those proteins containing a functional NLS are able to facilitate yeast growth on media lacking histidine.

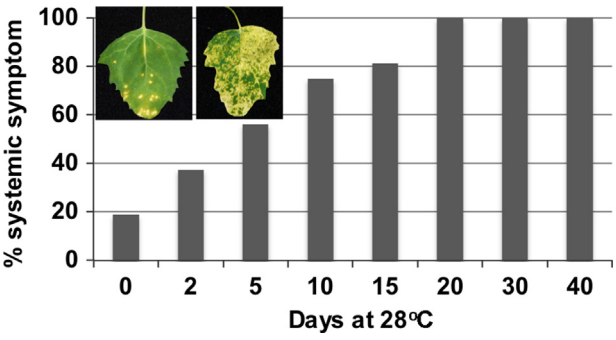

Fig. 11. Temperature-dependent systemic infection of *C. quinoa* by CoRSV. Uninoculated groups of plants ($n=18$) were incubated at 28 °C for various periods of time before inoculation with CoRSV. Post-inoculation plants were relocated to a greenhouse maintained at 24 °C and monitored for the appearance of systemic symptoms. Left inset: local lesions characteristic of inoculated leaves maintained at 24 °C. Right inset: symptoms of systemic CoRSV infections. This experiment was replicated three times.

Temperature-dependent expansion of CoRSV host range

CoRSV is difficult to maintain in coffee plants and so a number of experimental hosts have been identified (Chagas et al., 1981; Kitajima et al., 2011; Kitajima et al., 2010). Several of these species are commercially important crops or cosmopolitan weeds. Importantly, it is apparent that the host range of CoRSV can be influenced significantly by modest changes in temperature. In order to quantify this effect and to determine conditions that would facilitate consistent rates of susceptibility for this difficult-to-maintain virus, we conducted a time course series wherein *Chenopodium quinoa* plants were incubated at increasing periods of time at 28 °C before challenge with CoRSV, followed by maintenance of the plants at 24 °C (Fig. 11). Plants maintained at 24 °C developed only local lesions in inoculated leaves. However, there was a time-dependent increase in the percentage of plants that developed systemic susceptibility following modest lengths of incubation at 28 °C. Past 15 days at 28 °C, plants showed universal susceptibility to CoRSV.

Discussion

In this report we provide definitive molecular and microscopy-based characterization of the Lavras strain of CoRSV that removes any remaining ambiguity for inclusion of this virus in the recently proposed Dichorhavirus genus (Dietzgen et al., 2014). More importantly we have generated a wealth of information and resources that will serve as the foundation of future studies for the control of this emerging virus that is an increasing threat to coffee production and quality.

With regard to the nature of the encoded proteins, ORF1 shows homology to nucleocapsid proteins of rhabdoviruses, while ORF2 is similar to phosphoproteins. Consistent with N/P interactions for all plant-adapted rhabdoviruses tested to date and OFV, coexpression of these two proteins results in marked changes in their localization patterns. BiFC, which indicates primarily the localization of the most stable or abundant protein complex, showed that these proteins associate in the nucleus. However, coexpression of GFP and RFP fusions, which identifies both weak and strong interactions, showed that some ORF2p can be relocalized to the cytoplasm when in the presence of ORF1p. This suggests an interesting model for nuclear export of nucleocapsids, wherein the predicted NESs in ORF1p and ORF2p are in fact functional and can thus bind to nucleocapsids to mediate their transport from the nucleus. Nucleocapsids exported in this manner could then serve as a cell-to-cell movement complex (Cros and Palese, 2003; Min et al., 2010; O'Neill et al., 1998). ORF4p is likely the CoRSV matrix protein, which interacts with both ORF1p and ORF2p. The association of the ORF1p–ORF4p BiFC complex with perinuclear membranes suggests that this ORF4p may have some affinity for membranes, like the cognate proteins from SYNV and PYDV. The ORF5p protein localized exclusively to the nuclear envelope, consistent with predicted function as the CoRSV glycoprotein. Taken together, the nucleophilic character of the proteins encoded by ORFs 1, 2, 4, and 5 is consistent with their predicted roles in viroplasm formation and viral morphogenesis. In contrast, ORF3p localized strongly to the cell periphery, consistent with the localization patterns of SYNV-sc4, PYDV-Y and MFSV-3p, which are considered to be mediators of viral cell-to-cell movement. Although we were unable to localize the ORF6 protein, sequence analysis provided in Fig. 7 identifies all conserved hallmarks of rhabdoviral RNA-dependent RNA polymerases. Although OFV and CiLV-N were identical within the primary structure of the conserved polymerase motifs, CoRSV was divergent from these viruses in Motif D, suggesting a more distant relationship to OFV and CiLV-N, which are likely to be strains of the same virus.

In addition to their possible common ancestry and similar population genetics, determination of the CoRSV genome provides insight into mechanisms for transcriptional regulation in these viruses. Like OFV and CiLV-N, CoRSV particles in infected nuclei are roughly half the size of those of plant-adapted rhabdoviruses. This is considered to be a reflection that condensed nucleocapsid length is a function of the length of genomic RNAs, which are packaged independently. Shared with all members of the Mononegaviriales, the ORFs encoded by CoRSV are separated by tri-modular gene junctions. However, a curious distinction between OFV and CoRSV is that the leader/ORF1 and leader/ORF6 junctions in CoRSV are truncated and do not contain polyadenylation signals, instead only retaining the transcription start site, presumably used for ORF1 and ORF6 transcription. Therefore, we do not know at present if the leaders of CoRSV are transcribed and polyadenylated as they are in OFV (Kondo et al., 2014).

Of particular importance in guiding future studies derived from the present report is the ability of CoRSV to systemically infect initially resistant plants after exposure to increased temperatures. This has serious implications for expansion of virus reservoirs for this virus, particularly in light of predictions that global climatic change will severely and negatively impact coffee production and quality (Almeida et al., 2012; Bertrand et al., 2012; Davis et al., 2012; Gross, 2009). At present we do not know the molecular basis by which *C. quinoa* loses resistance CoRSV in response to elevated temperatures. However, similar phenomena have been characterized in other viral pathosystems. For example, the N gene-mediated resistance to *Tobacco mosaic virus* in *Nicotiana tabacum* is likewise ineffective when plants are maintained over 28 °C (Kiraly et al., 2008). Climate change, in contrast, will impose concomitant multifactorial effects on plants, which may result in synergistic physiological effects. In an elegant series of experiments,

Prasch and Sonnenwald demonstrated in an *Arabidopsis thaliana* model that simultaneous application of heat, drought and viral infection alters gene expression patterns in ways that cannot be predicted from single stress treatments (Prasch and Sonnewald, 2013). Interestingly, the enhanced expression of resistance genes typically observed in virus-infected plants was abolished in plants that were additionally stressed with heat and drought (Prasch and Sonnewald, 2013). Taken together, this and related research suggest that multiple signaling pathways are compromised under conditions that more closely simulate climate change. Relative to coffee production, modeling a 3 °C temperature increase based on recent reports from the International Panel on Climate Change (IPCC) suggests that Brazilian coffee production may result in the movement of coffee production from the MG state (14–23° parallel) to as far south as Rio Grande do Sul (26–34° parallel) (Zullo et al., 2011). Therefore, environmentally-mediated changes in the occurrence and host range of CoRSV, as suggested here with *C. quinoa*, should be an important focus for future research.

Although multifactorial interactions due to environmental effects are difficult to model, the projected situation for coffee can be exacerbated by the rise in the occurrence of CoRSV, which has emerged from an inconsequential virus when first discovered to be one of increasing incidents (Almeida et al., 2012; Bittancourt, 1938). Future studies will have to focus attention on the virus–vectors relationship for *B. phoenicis*-transmitted viruses that have bipartite or segmented genomes, as in the case of the dicorhavirus and emaravirus groups (Dietzgen et al., 2014; Elbeaino et al., 2009; Mielke-Ehret and Muhlbach, 2012). In a previous study of PYDV, we postulated, based upon L protein phylogenetics, that characteristics of the vector and not the host plant were the major determinants in evolution of plant-adapted rhabdoviruses (Bandyopadhyay et al., 2010). Given the close genetic relatedness between the nucleorhabdoviruses and dichroviruses, it is important to consider why the *B. phoenicis*-transmitted viruses considered in this study evolved to have segmented genomes. *B. phoenicis* populations are largely composed of sterile haploid females that reproduce clonally by parthenogenesis (Weeks et al., 2001). Males in these populations are produced only sporadically and likely are a minor contributor, if any, to sexual recombination in this species (Groot et al., 2005). A lack of genetic diversity in the vector population likely imposes severe restrictions on the ability of dichorhaviruses to recombine with genetically distinct strains. However, evolution to bipartite or multi-segmented species could facilitate genetic exchange by reassortment. While we favor the hypothesis that the most parsimonious evolutionary progression is from monopartite genomes to segmented forms, support for this is presently equivocal. However, the finding of very low genetic diversity within OFV populations is consistent with this hypothesis (Kubo et al., 2009).

In conclusion, we have provided a thorough characterization of the Lavras strain of CoRSV. The emergence and/or increased incidence of diseases of coffee have historically had severe socioeconomic impact (McCook, 2006; Ward, 1882). In this regard, the increased occurrence of CoRSV in all major coffee growing regions in Brazil is cause for global concern. Building from resources generated in this study, future research will map the genetic diversity within CoRSV populations as has been done for OFV (Kubo et al., 2009). Such research will help to determine the sustainability and utility of genetic resistance to CoRSV (Sera et al., 2013).

Materials and methods

Virus maintenance and purification

All plants, including transgenic *N. benthamiana* lines expressing autofluorescent proteins fused to histone 2B, a nuclear marker, were maintained in the greenhouse on open benches as described previously (Chakrabarty et al., 2007; Martin et al., 2009). CoRSV (strain Lavras; APHIS Permit P526P-12-04085) was maintained in *C. quinoa* at 28 °C in a locked environmental chamber or in insect-proof cages in a greenhouse under ambient conditions. Purification of CoRSV was done following the protocol of Chang et al. (1976), with modifications. Approximately 66 g of frozen *C. quinoa* leaves infected by CoRSV-Lavras, were macerated in 2 volumes (w/v) of 0.1 M phosphate buffer pH 7.0 with 0.01 M sodium diethyl carbamide, 0.1% ascorbic acid and 5% TritonX-100. The homogenate was clarified by centrifugation for 15 min at 3600*g*. The supernatant was centrifuged through a 20% sucrose pad for 3 h at 91,800*g*. Supernatant was discarded and the tube was rinsed thoroughly with ultrapure water to remove Triton excess. The resulting pellet was resuspended in 500 μl of 0.1 M phosphate buffer pH 7.0, tubes were sealed with parafilm and incubated overnight at 4 °C. The resuspended pellet was clarified by centrifugation at 7000*g* for 5 min. The final virus-containing suspension was stored at −80 °C.

Electron microscopy

Plant tissues were prepared for electron microscopy by fixation and embedding in Spurr resin (5 g vinylclohexene dioxide, 3 g of diglycidyl ether of propyleneglycol, 13 g of succine nonenyl anhydride and 0.2 g of dimethyl amino ethanol), essentially as described previously for examination of CoRSV in infected plant tissues (Kitajima et al., 2011). Prior to embedding strips of leaf tissue were fixed in a solution of 0.2 M cacodylate buffer containing 2% glutaraldehyde, 4% paraformaldehyde and 5 mM $CaCl_2$, for 4 h at 4 °C, followed by three sequential 10 min washes of 0.1 M cacodylate buffer. Fixed tissue was treated at 4 °C in 2% osmium tetroxide prepared in 0.2 M sodium phosphate buffer, pH 7.2, at room temperature for 1 h. The tissue was then transferred to a 2% uranyl acetate solution and incubated overnight. Following three 5 min washes in 0.9% saline, the tissue was dehydrated with a series of increasing concentrations of acetone: 25%, 50% and 70% for 5 min each and after that in 90% acetone for 10 min, and finally for 20 min with pure acetone for three times. Dehydrated tissue was infiltated with Spurr resin dissolved in acetone in the following manner, Spurr+acetone (1:1 ratio) at room temperature for 3 h, Spurr dissolved in acetone (2:1 ratio) at room temperature 3 h and a final overnight incubation at 4 °C. Finally, fixed tissue was placed into rubber molds filled with Spurr resin and incubated in an oven at 80 °C for 12 h to allow polymerization of the resin. Ultra-thin sections were obtained with an ultramicrotome (Reichert-Jung) and placed on 400-mesh copper grids, treated previously with metallic colloid and carbon. Sections were treated with 3% uranyl acetate for 20 min to enhance contrast and then washed with double-distilled water and contrasted with 0.4% lead citrate for 10 min, and rinsed with double-distilled water prior to examination under a Zeiss EM-109 transmission electron microscope.

Isolation of total RNA, RT-PCR

Total RNA was extracted from plant tissues using the Qiagen RNeasy Plant minikit according to the manufacturer's instructions (Qiagen). Except where noted, first strand cDNA synthesis and polymerase chain reactions (PCRs) were carried out using Superscript reverse transcriptase III (Invitrogen) and Phusion high fidelity DNA polymerase (Finnzymes), respectively.

Rapid amplification of cDNA ends (RACE)

Multiple methods were used to ensure capture of the bona fide termini of CoRSV genomic RNAs. 3′- and 5′-RACE was performed

with the BD-SMART RACE cDNA Amplification kit according to the manufacturer's instructions (Clontech) or the poly-adenylation method utilized by the RACE kits from Ambion. For these analyses, cDNA was synthesized by MMLV reverse transcriptase, and PCRs were conducted with Advantage-II DNA polymerase (Clontech).

ION Torrent sequencing

ION Torrent sequencing was performed by the staff of the Advanced Genetic Technology Center (University of Kentucky). Poly(A)$^+$-RNA was purified from total RNA isolated from CoRSV-infected *C. quinoa* leaves using a Dynabeads mRNA Purification Kit according to the manufacturer's instructions. Template cDNA was prepared using an IonPGM Template OT (One-Touch) 200 Kit. Sequencing was performed with an Ion PGM Sequencing 200 Kit and the Ion 316 chip. A total of 379.98 Mbp of sequence was generated of which 294.07 Mbp was considered high quality (Q_{20}), with read lengths in the range of 65–382 bp. Contigs were assembled from the high quality read data using the Trinity assembler package (Haas et al., 2013).

Phylogenetic analysis

All L protein sequences used in the sequence alignment study were obtained from data deposited in the NCBI database. The deduced amino acid sequences of the L genes were aligned using the CLUSTAL W algorithm (Larkin et al., 2007; Thompson et al., 1994) included in the MegAlign program of the DNASTAR software package. The alignments were analyzed by MEGA4.0.2 (Tamura et al., 2007). The phylogenetic tree derived from these datasets was generated using the neighbor-joining method (Saitou and Nei, 1987) with a bootstrap test with 1000 replicates to determine the percentage of replicate trees in which the taxa were clustered together. The evolutionary relationship of these polymerase proteins was computed using the Dayhoff matrix-based method. In contrast to other algorithms for determining phylogenetic relationships, the Dayhoff method is more effective when using small datasets of closely related proteins, which is the assumption made here as dichoraviruses and nucleorhabdoviruses are hypothesized to share a common ancestry (Dietzgen et al., 2014; Kondo et al., 2006). L gene sequences utilized in phylogenetic analyses include the following: CoRSV (KF812526.1), orchid fleck virus (OFV; NC_009609.1), citrus leprosis virus nuclear type (CiLV-N; AGN91973), *Lettuce necrotic yellows virus* (LNYV; AJ867584), *Vesicular stomatitis Indiana virus* (VSIV; NC_001560.1), *Maize mosaic virus* (MMV; AY618418.1), *Sonchus yellow net virus* (SYNV; L32603.1), *Maize fine streak virus* (MFSV; AY618417.1), *Potato yellow dwarf virus* (PYDV; NC_016136.1), *Maize Iranian mosaic virus* (MIMV; DQ186554) and *Strawberry crinkle virus* (SCV; AY2-50986.2). In addition, the sequences for *Rice yellow stunt virus* (RYSV; NC_003746.1), *Taro vein chlorosis* (TaVCV; NC_006942.1) and *Northern cereal mosaic virus* (NCMV; NC_002251.1) were used for the analyses of intergenic junctions and terminal sequences.

Protein expression in plant cells

Sequence-validated clones in vector pDONR221 (Invitrogen) of all CoRSV ORFs encoded by RNA1 were recombined into appropriate binary vectors for the expression of autofluorescent protein fusions in plant cells for localization and bimolecular fluorescence complementation (BiFC) assays as described previously (Chakrabarty et al., 2007; Martin et al., 2009). Vectors employed in this study were pSITE-2CA , pSITE-2NB (GFP fusions) and pSITEII-6C1 (TagRFP fusions) for localization experiments, and the pSITE-BiFC-nEYFP and pSITE-BiFC-cEYFP vectors for BiFC assays (Chakrabarty et al., 2007; Martin et al., 2009). Recombinant vectors were transformed into *Agrobacterium tumefaciens* strain LBA4404. Agroinfiltration for expression of protein fusions in plant cells was conducted essentially as described previously (Goodin et al., 2007). Each expression construct was examined in sections taken from a minimum of three leaves from each of three independent plants (nine leaves total). Several hundred cells were examined for each experiment and at least six high-resolution micrographs were acquired for each construct.

Laser scanning confocal microscopy

All microscopies were performed on an Olympus FV1000 laser-scanning confocal microscope as described previously (Goodin et al., 2005, 2007; Martin et al., 2009).

Nuclear import assays in yeast cells

We have previously adapted pNIAc to accommodate Gateway recombination-based cloning (Bandyopadhyay et al., 2010; Zaltsman et al., 2007). Recombinant pNIA-DEST plasmids for expression of CoRSV ORFs 1–5, as well as clones of maltose-binding protein (MBP) and histone 2B, were transformed into *Saccharomyces cerevisiae* strain L40 (Zaltsman et al., 2007). The transformed yeast cells were grown for 2 days at 30 °C on minimal media lacking tryptophan (Trp$^-$). Yeast colonies were then re-streaked onto minimal media lacking both tryptophan and histidine (His$^-$) and containing 5 mM 3-amino-1,2,4,-triazole (3AT). Growth of yeast cultures on Trp$^-$/His$^-$ media was indicative of a functional nuclear localization signal in proteins expressed from pNIA-DEST (Anderson et al., 2012; Bandyopadhyay et al., 2010).

Acknowledgments

We thank the CNPq, CAPES, FAPEMIG, and NSF funding agencies for providing research grants to M.G. and A.F. We would also like to thank the farmers and Cooperative workers who graciously provided access to their farms in support of this research (CAPES Project No. A009, 1901133, and NSF-IOS-0749519). We wish to thank John Shaw and David Smith for critical reading of the manuscript prior to submission. Finally we wish to thank David Zaitlin at the Kentucky Tobacco Research & Development Center for providing access to growth chambers critical to experiments conducted for this manuscript.

References

Almeida, J.E.M., Mori, A.E., Pozza, E.A., Reis, P.R., Figueira, A.D., 2012. Temporal analysis and control of the ringspot disease and mite vector of Coffee ringspot virus. Pesqui. Agropecu. Bras. 47, 913–919.

Anderson, G., Wang, R., Bandyopadhyay, A., Goodin, M., 2012. The nucleocapsid protein of Potato yellow dwarf virus: protein interactions and nuclear import mediated by a non-canonical nuclear localization signal. Front. Plant Sci. 3, 14.

Bandyopadhyay, A., Kopperud, K., Anderson, G., Martin, K., Goodin, M., 2010. An integrated protein localization and interaction map for Potato yellow dwarf virus, type species of the genus Nucleorhabdovirus. Virology 402, 61–71.

Bendtsen, J.D., Nielsen, H., von Heijne, G., Brunak, S., 2004. Improved prediction of signal peptides: signalP 3.0. J. Mol. Biol. 340, 783–795.

Bertrand, B., Boulanger, R., Dussert, S., Ribeyre, F., Berthiot, L., Descroix, F., Joet, T., 2012. Climatic factors directly impact the volatile organic compound fingerprint in green Arabica coffee bean as well as coffee beverage quality. Food Chem. 135, 2575–2583.

Bittancourt, A.A., 1938. A mancha anular, uma nova ameaça do cafeeiro. O Biol. 4, 404–405.

Blom, M.L., Green, W.R., Schachat, A.P., 1994. Diabetic retinopathy: a review. Del. Med. J. 66, 379–388.

Blom, N., Sicheritz-Ponten, T., Gupta, R., Gammeltoft, S., Brunak, S., 2004. Prediction of post-translational glycosylation and phosphorylation of proteins from the amino acid sequence. Proteomics 4, 1633–1649.

Bourhy, H., Cowley, J.A., Larrous, F., Holmes, E.C., Walker, P.J., 2005. Phylogenetic relationships among rhabdoviruses inferred using the L polymerase gene. J. Gen. Virol. 86, 2849–2858.
Chagas, C.M., July, J.R., Alba, A.P.C, 1981. Mechanical transmission and structural features of Coffee ringspot virus (Crv). Phytopathol. Z. 102, 100–106.
Chagas, C.M., Kitajima, E.W., Rodrigues, J.C., 2003a. Coffee ringspot virus vectored by Brevipalpus phoenicis (Acari: Tenuipalpidae) in coffee. Exp. Appl. Acarol. 30, 203–213.
Chagas, C.M., Kitajima, E.W., Rodrigues, J.C.V., 2003b. Coffee ringspot virus vectored by Brevipalpus phoenicis (Acari: Tenuipalpidae) in coffee. Exp. Appl. Acarol. 30, 203–213.
Chakrabarty, R., Banerjee, R., Chung, S.M., Farman, M., Citovsky, V., Hogenhout, S.A., Tzfira, T., Goodin, M., 2007. PSITE vectors for stable integration or transient expression of autofluorescent protein fusions in plants: probing Nicotiana benthamiana-virus interactions. Mol. Plant-Microbe Interact. 20, 740–750.
Chang, M.U., Arai, K., Doi, Y., Yora, K., 1976. Morphology and intracellular appearance of orchid fleck virus. Ann. Phytopath. Soc. Jpn. 42, 156–157.
Coetzee, B., Freeborough, M.J., Maree, H.J., Celton, J.M., Rees, D.J., Burger, J.T., 2010. Deep sequencing analysis of viruses infecting grapevines: virome of a vineyard. Virology 400, 157–163.
Cros, J.F., Palese, P., 2003. Trafficking of viral genomic RNA into and out of the nucleus: influenza, Thogoto and Borna disease viruses. Virus Res. 95, 3–12.
Davis, A.P., Gole, T.W., Baena, S., Moat, J., 2012. The impact of climate change on indigenous Arabica coffee (Coffea arabica): predicting future trends and identifying priorities. PloS One 7, e47981.
De Carvalho Mineiro, J.L., Sato, M.E., Raga, A., Arthur, V., 2008. Population dynamics of phytophagous and predaceous mites on coffee in Brazil, with emphasis on Brevipalpus phoenicis (Acari: Tenuipalpidae). Exp. Appl. Acarol. 44, 277–291.
Deng, M., Bragg, J.N., Ruzin, S., Schichnes, D., King, D., Goodin, M.M., Jackson, A.O., 2007. Role of the sonchus yellow net virus N protein in formation of nuclear viroplasms. J. Virol. 81, 5362–5374.
Dietzgen, R.G., Kuhn, J.H., Clawson, A.N., Freitas-Astua, J., Goodin, M.M., Kitajima, E.W., Kondo, H., Wetzel, T., Whitfield, A.E., 2014. Dichorhavirus: a proposed new genus for Brevipalpus mite-transmitted, nuclear, bacilliform, bipartite, negative-strand RNA plant viruses. Arch. Virol. 159, 607–619.
Elbeaino, T., Digiaro, M., Martelli, G.P., 2009. Complete nucleotide sequence of four RNA segments of fig mosaic virus. Arch. Virol. 154, 1719–1727.
Elton, D., Simpson-Holley, M., Archer, K., Medcalf, L., Hallam, R., McCauley, J., Digard, P., 2001. Interaction of the influenza virus nucleoprotein with the cellular CRM1-mediated nuclear export pathway. J. Virol. 75, 408–419.
Figueira, A.R., 2008. A mancha anelar do cafeeiro causada pelo Coffee ringspot virus (CoRSV) em Minas Gerais. Núcleo de Estudos em Fitopatologia; Universidade Federal de Lavras. (Org.). Manejo fitossanitário da cultura do cafeeiro. Sociedade Brasileira de Fitopatologia, Brasília, DF, Brasil, 127–139.
Gasteiger, E., Gattiker, A., Hoogland, C., Ivanyi, I., Appel, R.D., Bairoch, A., 2003. ExPASy: the proteomics server for in-depth protein knowledge and analysis. Nucleic Acids Res. 31, 3784–3788.
Gaudin, Y., Ruigrok, R.W., Tuffereau, C., Knossow, M., Flamand, A., 1992. Rabies virus glycoprotein is a trimer. Virology 187, 627–632.
Ghosh, D., Brooks, R.E., Wang, R., Lesnaw, J., Goodin, M.M., 2008. Cloning and subcellular localization of the phosphoprotein and nucleocapsid proteins of Potato yellow dwarf virus, type species of the genus Nucleorhabdovirus. Virus Res. 135, 26–35.
Goodin, M., Yelton, S., Ghosh, D., Mathews, S., Lesnaw, J., 2005. Live-cell imaging of rhabdovirus-induced morphological changes in plant nuclear membranes. Mol. Plant-Microbe Interact. 18, 703–709.
Goodin, M.M., Austin, J., Tobias, R., Fujita, M., Morales, C., Jackson, A.O., 2001. Interactions and nuclear import of the N and P proteins of sonchus yellow net virus, a plant nucleorhabdovirus. J. Virol. 75, 9393–9406.
Goodin, M.M., Chakrabarty, R., Yelton, S., Martin, K., Clark, A., Brooks, R., 2007. Membrane and protein dynamics in live plant nuclei infected with Sonchus yellow net virus, a plant-adapted rhabdovirus. J. Gen. Virol. 88, 1810–1820.
Grard, G., Fair, J.N., Lee, D., Slikas, E., Steffen, I., Muyembe, J.J., Sittler, T., Veeraraghavan, N., Ruby, J.G., Wang, C., Makuwa, M., Mulembakani, P., Tesh, R.B., Mazet, J., Rimoin, A.W., Taylor, T., Schneider, B.S., Simmons, G., Delwart, E., Wolfe, N.D., Chiu, C.Y., Leroy, E.M., 2012. A novel rhabdovirus associated with acute hemorrhagic fever in central Africa. PLoS Pathog. 8, e1002924.
Groot, T.V., Janssen, A., Pallini, A., Breeuwer, J.A., 2005. Adaptation in the asexual false spider mite Brevipalpus phoenicis: evidence for frozen niche variation. Exp. Appl. Acarol. 36, 165–176.
Gross, M., 2009. Coffee growers feel the heat. Curr. Biol. 19, R965–R966.
Haas, B.J., Papanicolaou, A., Yassour, M., Grabherr, M., Blood, P.D., Bowden, J., Couger, M.B., Eccles, D., Li, B., Lieber, M., Macmanes, M.D., Ott, M., Orvis, J., Pochet, N., Strozzi, F., Weeks, N., Westerman, R., William, T., Dewey, C.N., Henschel, R., Leduc, R.D., Friedman, N., Regev, A., 2013. De novo transcript sequence reconstruction from RNA-seq using the Trinity platform for reference generation and analysis. Nat. Protoc. 8, 1494–1512.
Idris, A., Al-Saleh, M., Piatek, M.J., Al-Shahwan, I., Ali, S., Brown, J.K., 2014. Viral metagenomics: analysis of begomoviruses by illumina high-throughput sequencing. Viruses 6, 1219–1236.
Ito, T., Suzaki, K., Nakano, M., 2013. Genetic characterization of novel putative rhabdovirus and dsRNA virus from Japanese persimmon. J. Gen. Virol. 94, 1917–1921.
Jackson, A.O., Dietzgen, R.G., Goodin, M.M., Bragg, J.N., Deng, M., 2005. Biology of plant rhabdoviruses. Annu. Rev. Phytopathol. 43, 623–660.
Kerppola, T.K., 2008. Bimolecular fluorescence complementation (BiFC) analysis as a probe of protein interactions in living cells. Annu. Rev. Biophys. 37, 465–487.
Kiraly, L., Hafez, Y.M., Fodor, J., Kiraly, Z., 2008. Suppression of tobacco mosaic virus-induced hypersensitive-type necrotization in tobacco at high temperature is associated with downregulation of NADPH oxidase and superoxide and stimulation of dehydroascorbate reductase. J. Gen. Virol. 89, 799–808.
Kitajima, E.W., Chagas, C.M., Braghini, M.T., Fazuoli, L.C., Locali-Fabris, E.C., Salaroli, R.B., 2011. Natural infection of several Coffea species and hybrids and Psilanthus ebracteolatus by the Coffee ringspot virus (CoRSV). Sci. Agric. 68, 503–507.
Kitajima, E.W., Chagas, C.M., Rodrigues, J.C., 2003a. Brevipalpus-transmitted plant virus and virus-like diseases: cytopathology and some recent cases. Exp. Appl. Acarol. 30, 135–160.
Kitajima, E.W., Chagas, C.M., Rodrigues, J.C.V., 2003b. Brevipalpus-transmitted plant virus and virus-like diseases: cytopathology and some recent cases. Exp. Appl. Acarol. 30, 135–160.
Kitajima, E.W., Rodrigues, J.C.V., Freitas-Astua, J., 2010. An annotated list of ornamentals naturally found infected by Brevipalpus mite-transmitted viruses. Sci. Agric. 67, 348–371.
Kondo, H., Chiba, S., Andika, I.B., Maruyama, K., Tamada, T., Suzuki, N., 2013. Orchid fleck virus structural proteins N and P form intranuclear viroplasm-like structures in the absence of viral infection. J. Virol. 87, 7423–7434.
Kondo, H., Maeda, T., Shirako, Y., Tamada, T., 2006. Orchid fleck virus is a rhabdovirus with an unusual bipartite genome. J. Gen. Virol. 87, 2413–2421.
Kondo, H., Maeda, T., Tamada, T., 2009. Identification and characterization of structural proteins of orchid fleck virus. Arch. Virol. 154, 37–45.
Kondo, H., Maruyama, K., Chiba, S., Andika, I.B., Suzuki, N., 2014. Transcriptional mapping of the messenger and leader RNAs of orchid fleck virus, a bisegmented negative-strand RNA virus. Virology 452-453, 166–174.
Kreis, T.E., Lodish, H.F., 1986. Oligomerization is essential for transport of vesicular stomatitis viral glycoprotein to the cell surface. Cell 46, 929–937.
Kubo, K.S., Stuart, R.M., Freitas-Astua, J., Antonioli-Luizon, R., Locali-Fabris, E.C., Coletta-Filho, H.D., Machado, M.A., Kitajima, E.W., 2009. Evaluation of the genetic variability of orchid fleck virus by single-strand conformational polymorphism analysis and nucleotide sequencing of a fragment from the nucleocapsid gene. Arch. Virol. 154, 1009–1014.
Larkin, M.A., Blackshields, G., Brown, N.P., Chenna, R., McGettigan, P.A., McWilliam, H., Valentin, F., Wallace, I.M., Wilm, A., Lopez, R., Thompson, J.D., Gibson, T.J., Higgins, D.G., 2007. Clustal W and Clustal X version 2.0. Bioinformatics 23, 2947–2948.
Martin, K., Kopperud, K., Chakrabarty, R., Banerjee, R., Brooks, R., Goodin, M.M., 2009. Transient expression in Nicotiana benthamiana fluorescent marker lines provides enhanced definition of protein localization, movement and interactions in planta. Plant J. 59, 150–162.
Martin, K.M., Dietzgen, R.G., Wang, R., Goodin, M.M., 2012. Lettuce necrotic yellows cytorhabdovirus protein localization and interaction map, and comparison with nucleorhabdoviruses. J. Gen. Virol. 93, 906–914.
McCook, S., 2006. Global rust belt: Hemileia vastatrix and the ecological integration of world coffee production since 1850. J. Global Hist. 1, 177–195.
Mielke-Ehret, N., Muhlbach, H.P., 2012. Emaravirus: a novel genus of multipartite, negative strand RNA plant viruses. Viruses 4, 1515–1536.
Min, B.E., Martin, K., Wang, R., Tafelmeyer, P., Bridges, M., Goodin, M., 2010. A host-factor interaction and localization map for a plant-adapted rhabdovirus implicates cytoplasm-tethered transcription activators in cell-to-cell movement. Mol. Plant-Microbe Interact. 23, 1420–1432.
Nakai, K., Kanehisa, M., 1991. Expert system for predicting protein localization sites in gram-negative bacteria. Proteins 11, 95–110.
Nakai, K., Kanehisa, M., 1992. A knowledge base for predicting protein localization sites in eukaryotic cells. Genomics 14, 897–911.
Nunes, M.A., Lameiro, P., Calegario, R.F., Bergamini, M.P., Coerini, L.F., Kitajima, E.W., Bastianel, M., Novelli, V.M., Freitas-Astúa, J., 2012. Trapoeraba (Commelina benghalensis L.) como fonte de inóculo do vírus da leprose dos citros. Citrus Res. Technol. 33, 1–9.
O'Neill, R.E., Talon, J., Palese, P., 1998. The influenza virus NEP (NS2 protein) mediates the nuclear export of viral ribonucleoproteins. EMBO J. 17, 288–296.
Prasch, C.M., Sonnewald, U., 2013. Simultaneous application of heat, drought, and virus to Arabidopsis plants reveals significant shifts in signaling networks. Plant Physiol. 162, 1849–1866.
Saitou, N., Nei, M., 1987. The neighbor-joining method: a new method for reconstructing phylogenetic trees. Mol. Biol. Evol. 4, 406–425.
Sera, T., Sera, G.H., Fazuoli, L.C., Bettencourt, A.J., 2013. IPR 99-Dwarf arabica coffee cultivar resistant to coffee ringspot virus. Crop Breed. Appl. Biotechnol. 13, 91–94.
Tamura, K., Dudley, J., Nei, M., Kumar, S., 2007. MEGA4: Molecular Evolutionary Genetics Analysis (MEGA) software version 4.0. Mol. Biol. Evol. 24, 1596–1599.
Thompson, J.D., Higgins, D.G., Gibson, T.J., 1994. CLUSTAL W: improving the sensitivity of progressive multiple sequence alignment through sequence weighting, position-specific gap penalties and weight matrix choice. Nucleic Acids Res. 22, 4673–4680.
Tsai, C.W., Redinbaugh, M.G., Willie, K.J., Reed, S., Goodin, M., Hogenhout, S.A., 2005. Complete genome sequence and in planta subcellular localization of maize fine streak virus proteins. J. Virol. 79, 5304–5314.
Vives, M.C., Velazquez, K., Pina, J.A., Moreno, P., Guerri, J., Navarro, L., 2013. Identification of a new enamovirus associated with citrus vein enation disease by deep sequencing of small RNAs. Phytopathology 103, 1077–1086.

Ward, M.H., 1882. On the morphology of Hemileia vastatrix Berk. & Br. (The fungus of the coffee disease of Ceylon). Q. J. Microsc. Sci. 22, 1–11.
Weeks, A.R., Marec, F., Breeuwer, J.A., 2001. A mite species that consists entirely of haploid females. Science 292, 2479–2482.
Wetzel, T., Dietzgen, R.G., Dale, J.L., 1994. Genomic organization of lettuce necrotic yellows rhabdovirus. Virology 200, 401–412.
Whitt, M.A., Buonocore, L., Prehaud, C., Rose, J.K., 1991. Membrane fusion activity, oligomerization, and assembly of the rabies virus glycoprotein. Virology 185, 681–688.
Wilcox, M.D., McKenzie, M.O., Parce, J.W., Lyles, D.S., 1992. Subunit interactions of vesicular stomatitis virus envelope glycoprotein influenced by detergent micelles and lipid bilayers. Biochemistry 31, 10458–10464.
Zaltsman, A., Yi, B.Y., Krichevsky, A., Gafni, Y., Citovsky, V., 2007. Yeast-plant coupled vector system for identification of nuclear proteins. Plant Physiol. 145, 1264–1271.
Zullo, J., Pinto, H.S., Assad, E.D., de Avila, A.M.H., 2011. Potential for growing Arabica coffee in the extreme south of Brazil in a warmer world. Clim. Change 109, 535–548.